Binary Alkali-Metal Silicon Clathrates by Spark Plasma Sintering: Preparation and Characterization

Igor Veremchuk [1], Matt Beekman [2], Iryna Antonyshyn [1], Walter Schnelle [1], Michael Baitinger [1], George S. Nolas [3],* and Yuri Grin [1],*

[1] Max-Planck-Institut für Chemische Physik fester Stoffe, 01187 Dresden, Germany;
     Igor.Veremchuk@cpfs.mpg.de (I.V.); Iryna.Antonyshyn@cpfs.mpg.de (I.A.);
     Walter.Schnelle@cpfs.mpg.de (W.S.); Michael.Baitinger@cpfs.mpg.de (M.B.)
[2] Department of Physics, California Polytechnic State University, San Luis Obispo, CA 93407, USA;
     mbeekman@calpoly.edu
[3] Department of Physics, University of South Florida, Tampa, FL 33620, USA
*   Correspondence: gnolas@cas.usf.edu (G.S.N.); grin@cpfs.mpg.de (Y.G.);
     Tel.: +1-813-974-2233 (G.S.N.); +49-351-46464000 (Y.G.)

Abstract: The binary intermetallic clathrates $K_{8-x}Si_{46}$ (x = 0.4; 1.2), $Rb_{6.2}Si_{46}$, $Rb_{11.5}Si_{136}$ and $Cs_{7.8}Si_{136}$ were prepared from M_4Si_4 (M = K, Rb, Cs) precursors by spark-plasma route (SPS) and structurally characterized by Rietveld refinement of PXRD data. The clathrate-II phase $Rb_{11.5}Si_{136}$ was synthesized for the first time. Partial crystallographic site occupancy of the alkali metals, particularly for the smaller Si_{20} dodecahedra, was found in all compounds. SPS preparation of $Na_{24}Si_{136}$ with different SPS current polarities and tooling were performed in order to investigate the role of the electric field on clathrate formation. The electrical and thermal transport properties of $K_{7.6}Si_{46}$ and $K_{6.8}Si_{46}$ in the temperature range 4–700 K were investigated. Our findings demonstrate that SPS is a novel tool for the synthesis of intermetallic clathrate phases that are not easily accessible by conventional synthesis techniques.

Keywords: spark plasma synthesis; Zintl phase; intermetallic clathrate

1. Introduction

Binary phases of alkali metals with silicon have been prepared by thermal decomposition of the monosilicides M_4Si_4 (M = Na, K, Rb, Cs) for over six decades [1–4]. Structural investigations of the polycrystalline products revealed the existence of clathrate-I $M_{8-x}Si_{46}$ and clathrate-II $M_{24-x}Si_{136}$ silicides [5,6]. In both clathrate types, the alkali-metal atoms are enclosed in polyhedral cages formed in the tetrahedrally bonded silicon framework. In the clathrate-I crystal structure, the unit cell contains two Si_{20} and six Si_{24} cages, while in the clathrate-II structure there are sixteen Si_{20} and eight Si_{28} cages present in the unit cell. In the clathrate phases prepared by thermal decomposition the filling fraction of M in the silicon cages depends explicitly on both the reaction conditions and the size of the M atom relative to the size of the cage [6] (Figure 1).

Alternatively, redox techniques have been developed to obtain metastable clathrate phases [7–10] including Ge and Si allotropes with empty cages [11,12]. Defect-free single crystals of alkali metal silicon clathrates large enough for structure investigations have only been obtained in exceptional cases [4]. For example, crystals of K_8Si_{46} were grown on α-Si exposed to potassium vapor [13], while crystals of ternary clathrate-II phases $Rb_8Na_{16}Si_{136}$ and $Cs_8Na_{16}Si_{136}$ form in closed ampoules directly from the melt [14,15]. Single-crystals suitable for measurement of intrinsic transport properties were first prepared by the electrochemically-driven transformation of Na_4Si_4 to $Na_{24}Si_{136}$

during the spark plasma treatment (SPS) [16,17]. Another approach—the kinetically controlled thermal decomposition (KCTD) method—can also provide relatively large single crystals [18,19]. Recently, a thermal decomposition at lower temperatures was employed for the preparation of $Na_{24-x}(Si_yGe_{1-y})_{136}$ and proved to be useful for the synthesis of silicon clathrates [20]. Extensions of the SPS and KCTD approaches have also recently reported, including use of multi-phase precursors or simultaneous ion-exchange and electrochemical reactions to prepare ternary or quaternary clathrates [21–23].
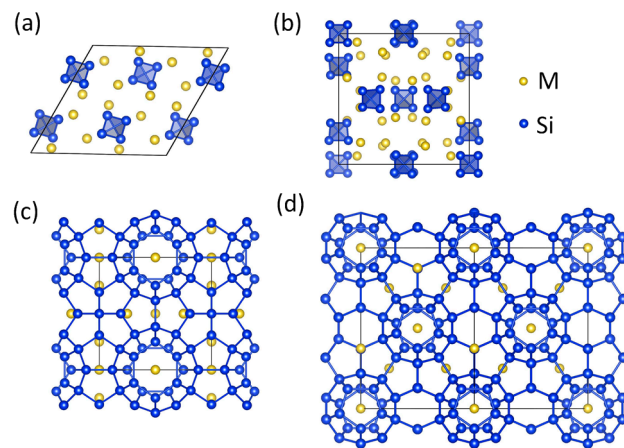
Figure 1. Crystal structures of (**a**) Na_4Si_4; (**b**) M_4Si_4 (M = K, Rb, or Cs); (**c**) $M_{8-x}Si_{46}$; and (**d**) $M_{24-x}Si_{136}$.

The unique advantage of SPS for the synthesis of clathrates by producing scalable, compact bulk materials also continues to be of great interest [4]. In this work we discuss both the preparation and consolidation of alkali-metal silicon clathrates by SPS. We report on the preparation and crystal structure of different clathrate phases (Table 1) as well as SPS densification of $K_{7.6}Si_{46}$ and $K_{6.8}Si_{46}$ powders by SPS that allow for the investigation of their transport properties over a large temperature range. The formation and evaporation the free alkali metals during the reaction allow us to work only with a small amount (less than 200 mg) of precursors and, in the results, after processing, we obtained 10–20 mg of the materials.

Table 1. Spark-plasma synthesis (SPS) conditions for the silicon clathrates.

Precursor	T_R (°C) [a]	t_R (min) [b]	Die/Punches [c]	Products [d]
Na_4Si_4	550	180	C/C	$Na_{24}Si_{136}$ (M) + Na_8Si_{46} (m)
	600	180	C/C	$Na_{24}Si_{136}$ (M)
	700	180	C/C	$Na_{24}Si_{136}$ (M) + Si (m)
K_4Si_4	500	60	BN/SS	$K_{8-x}Si_{46}$ (tr)
	550	60	BN/SS	$K_{8-x}Si_{46}$ (M)
	600	60	BN/SS	$K_{8-x}Si_{46}$ (M) + Si (m)
	650	60	BN/SS	Si (M) + $K_{8-x}Si_{46}$ (m)
Rb_4Si_4	450	60	BN/SS	$Rb_{8-x}Si_{46}$ (M) + $Rb_{24-x}Si_{136}$ (m) + Si (tr)
	500	60	BN/SS	Si (M) + $Rb_{8-x}Si_{46}$ (m) + $Rb_{24-x}Si_{136}$ (m)
Cs_4Si_4	350	60	BN/SS	$Cs_{8-x}Si_{136}$ (M) + Si (tr)

[a] T_R is the reaction temperature; [b] t_R is the treatment time; [c] Materials for the die and punches: C = graphite, BN = *hp*-boron nitride, SS = stainless steel; [d] Excluding unreacted precursor. M = majority phase, m = minority phase, tr = trace.

2. Results and Discussion

As first described in reference [16], clathrates are formed during SPS redox-treatment by oxidation of $Si_4{}^{4-}$ at the anode while the alkali metal is reduced at the cathode (Figure 2a,b). Clathrate-II formation, according to

$$34\,M_4Si_4 \rightarrow M_{24}Si_{136} \,+\, 112\,M$$
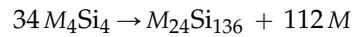
can therefore be described by the half-reactions

$$34\,Si_4{}^{4-} - 112\,e^- \rightarrow Si_{136}{}^{24-} \ (anode)$$
$$112\,M^+ \,+\, 112\,e^- \rightarrow 112\,M^0 \ (cathode)$$

(1)
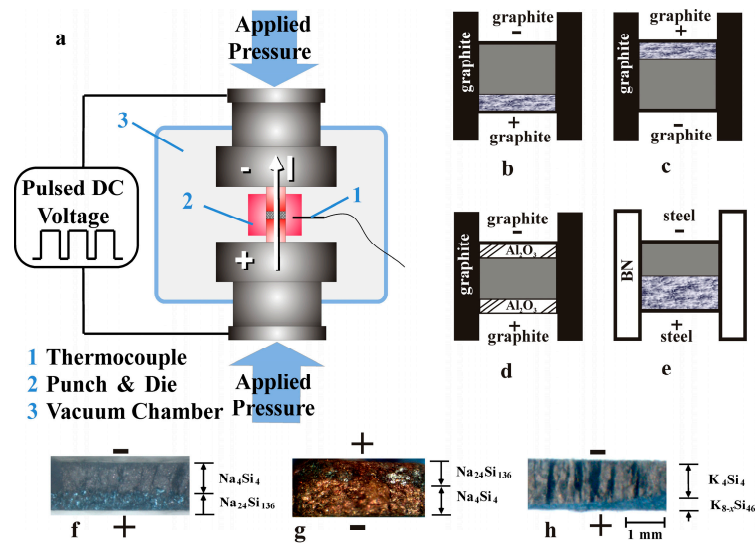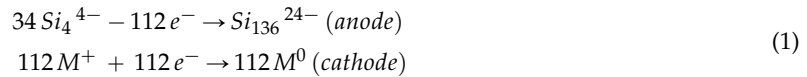
Figure 2. (**a**) SPS setup for the preparation of clathrates; (**b**–**e**) Location and relative amounts of the reaction products for different polarities and different die and punch materials; (**f**–**h**) Optical micrographs of the cross-sections from fractured post-reaction pellets illustrating the directional growth of clathrates at the anode.

For clathrate-I formation according to

$$23\,M_4Si_4 \rightarrow 2\,M_8Si_{46} \,+\, 76\,M$$

should be considered by means of the half-reactions

$$23\,Si_4{}^{4-} - 76\,e^- \rightarrow 2\,Si_{46}{}^{8-} \ (anode)$$
$$76\,M^+ \,+\, 76\,e^- \rightarrow 76\,M^0 \ (cathode)$$

(2)
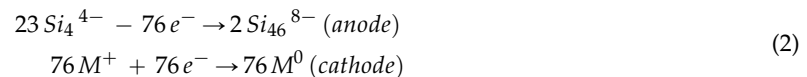
Reactions (1) and (2) describe the basics of the clathrate formation by SPS, whereby the process is driven by the DC field and the evaporation of the alkali metal at the cathode and its absorption by the graphite die (Figure 2b). In order to qualitatively investigate the influence of electric current on clathrate formation we performed three control experiments with Na_4Si_4 as the precursor. First, the polarity of the DC current was reversed, upon which it was found that the clathrate phase, $Na_{24}Si_{136}$ in this case, consistently forms at the anode (Figure 2c). In a second experiment, equal volumes of Al_2O_3 powder were placed above and below the precursor to create an electrically insulating barrier. The electrical current then presumably flowed through the low resistance graphite die such that the current passing through the Na_4Si_4 precursor is minimized. In this case no reaction was observed under the identical conditions used to form the clathrate $Na_{24}Si_{136}$ (Figure 2d). In the third experiment, the use of stainless steel punches combined with a die manufactured from boron nitride, a high electrical-resistivity material, presumably forced most of the current to pass through the precursor (as opposed to the

surrounding die) (Figure 2e). A more rapid reaction than in the case of using the graphite die was observed. Optical photographs of cross-section of SPS-processed pellets (Figure 2f,h) clearly show that formation of the clathrate phases occurred at the anode during SPS processing. This was also the case for all clathrate compositions prepared in this study.

The crystal structures of the SPS-prepared clathrate phases were investigated by the Rietveld method using powder X-ray diffraction (PXRD) data. Experimental, calculated, and difference diffraction patterns for the clathrate-I and II samples are shown on Figures 3 and 4, respectively, and the resulting crystallographic data are presented in Tables 2 and 3, respectively.
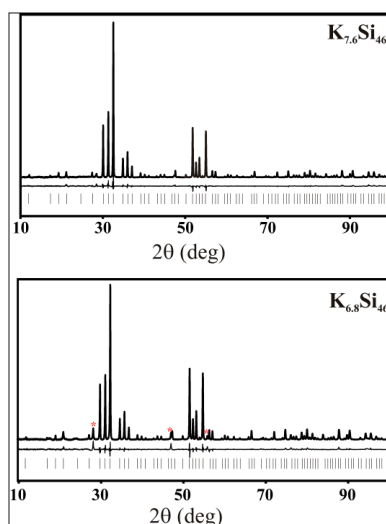
Figure 3. Powder X-ray diffraction (PXRD) patterns of the SPS-prepared clathrates-I $K_{7.6}Si_{46}$ (550 °C) and $K_{6.8}Si_{46}$ (600 °C). Red asterisks mark the reflections of α-Si (<0.2 mass % in $K_{7.6}Si_{46}$ and 1.5 mass % in $K_{6.8}Si_{46}$). The experimental intensities are shown as a solid line. The difference between the experimental and calculated intensities is shown below the experimental data; the tick marks represent the positions of the diffraction reflections of the clathrate-I phase.
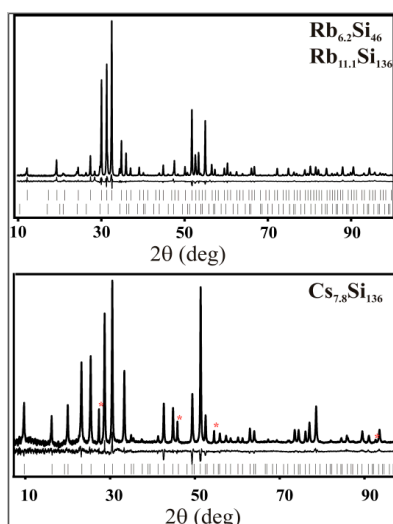
Figure 4. Powder X-ray diffraction (PXRD) patterns of the $Rb_{6.2}Si_{46}$ and $Rb_{11.1}Si_{136}$ mixed product and clathrate-II $Cs_{7.8}Si_{136}$. The experimental intensities are shown as a solid line. The differences between the experimental and calculated intensities are shown below the experimental data. The tick marks represent the positions of the diffraction reflections. Red asterisks mark the reflections from α-Si (<0.2 mass % in $Rb_{6.2}Si_{46}$ and $Rb_{11.1}Si_{136}$ and 2.5 mass % in $Cs_{7.8}Si_{136}$).

Table 2. Crystallographic information on the clathrate-I phases prepared by SPS (PXRD data).

Phase	$K_{7.6(1)}Si_{46}$	$K_{6.8(1)}Si_{46}$	$Rb_{6.2(1)}Si_{46}$
Lattice parameter a, Å	10.2776 (1)	10.2747 (1)	10.2848 (1)
Radiation, wavelength λ, Å		Cu $K_{\alpha1}$, 1.54056	
Maximal diffraction angle 2θ, °		100.30	
Residuals R_I/R_P	0.04/0.10	0.04/0.09	0.02/0.10
$M1$ $2a$ (0 0 0)	Occ * = 0.783 (1)	Occ = 0.695 (4)	Occ = 0.244 (3)
$M2$ $6d$ ($\frac{1}{4}$ $\frac{1}{2}$ 0)	Occ = 1.013 (3) **	Occ = 0.918 (3)	Occ = 0.961 (2)
Si1 $6c$ ($\frac{1}{4}$ 0 $\frac{1}{2}$)	–	–	–
Si2 $16i$ (x x x)	$x = 0.1845$ (1)	$x = 0.1846$ (1)	$x = 0.1840$ (1)
Si3 $24k$ (0 y z)	$y = 0.3068$ (1) $z = 0.1183$ (1)	$y = 0.3060$ (1) $z = 0.1185$ (1)	$y = 0.3043$ (1) $z = 0.1190$ (1)

*: Occ—occupancy factor; **: The value 1.013 (3) for the K2 occupancy in $K_{7.6}Si_{46}$ reflects the real error of the refinement ($\cong$4 e.s.d.) and helps to understand the reliability of the occupancy values for other clathrates.

Table 3. Crystallographic information on the clathrate-II phases prepared by SPS (PXRD data).

Phase	$Rb_{11.1(1)}Si_{136}$	$Cs_{7.8(1)}Si_{136}$
Lattice parameter a, Å	14.7142 (9)	14.6733 (3)
Radiation, wavelength λ, Å		Cu $K_{\alpha1}$, 1.54056
Maximal diffraction angle 2θ, °		100.30
Residuals R_I/R_P	0.10/0.10	0.05/0.13
$M1$ $8b$ (⅜ ⅜ ⅜)	Occ * = 0.85 (2)	Occ = 0.968 (2)
$M2$ $16c$ (0 0 0)	Occ = 0.272 (1)	Occ = 0.0
Si1 $8a$ (⅛ ⅛ ⅛)	–	–
Si2 $32e$ (x x x)	$x = 0.2198$ (6)	$x = 0.2168$ (2)
Si3 $96g$ (x x z)	$x = 0.1839$ (2) $z = 0.3698$ (6)	$x = 0.1822$ (1) $z = 0.3699$ (2)

*: Occ—occupancy factor.

　　The lattice parameters for $K_{7.6}Si_{46}$, $Rb_{6.2}Si_{46}$, and $Cs_{7.8}Si_{136}$ show good agreement with those synthesized by other preparation methods [7,16,18,19,24–26]. The lattice parameter for $Rb_{11.5}Si_{136}$, as expected, has an intermediate value between that reported for $K_{17.2}Si_{136}$ [19] and Cs_8Si_{136} [6]. In all cases the silicon framework sites were found to be fully occupied (no vacancies), in agreement with prior results for binary silicon clathrates [7,16,18,19,26–28]. The stable covalent Si–Si bonds in silicon clathrates allow for a large excess of electrons that fill antibonding states. In a rigid-band model, a high concentration of conduction electrons are provided by charge transfer from the alkali-metal guests, thus inducing metallic behavior, as confirmed experimentally [15,29]. In contrast to SPS-prepared Na_8Si_{46} and $Na_{24}Si_{136}$, which show full occupancy of the polyhedral cages by sodium [19], the SPS-prepared clathrates of potassium, rubidium and caesium exhibit partial occupancy of the alkali-atom positions (the specific refined compositions are given in Tables 2 and 3).

　　The compositions of clathrates-II prepared in this study together with previously reported in the literature [16,19,29,30] allow for a comparison of the lattice parameter versus guest-atom content in clathrate-II phases. As shown in Figure 5, in all cases the lattice parameter increases with those increasing M content in the Si_{20} (crystallographic site $16c$) cage. In addition, the lattice parameter also increases with increasing alkali-ion radius [31] for a specific M concentration. Preferential occupancy of the larger Si_{28} (crystallographic site $8b$) cages was observed for the case of $Rb_{11.5}Si_{136}$, as well as for for Na_xSi_{136} [30,32].
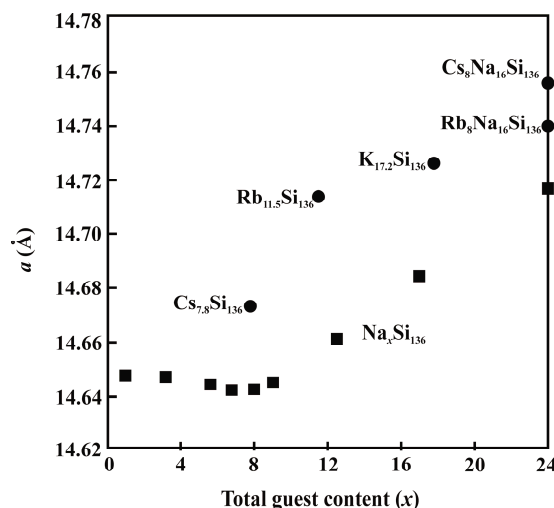
Figure 5. Lattice parameters versus *M* content, *x* for clathrate-I Na_xSi_{136} ($0 < x < 24$) [28], $Na_{24}Si_{136}$ [16], $K_{17.2}Si_{136}$ [19], $Rb_{11.5}Si_{136}$ (this work), and $Cs_{7.8}Si_{136}$ (this work), as well as ternary $Rb_8Na_{16}Si_{136}$ and $Cs_8Na_{16}Si_{136}$ [27].

In order to further characterize the products formed by SPS we measured the electrical and thermal transport properties of $K_{7.6}Si_{46}$ and $K_{6.8}Si_{46}$. The density of the pellets (only $K_{8-x}Si_{46}$) was approximately 90% of the calculated density based on PXRD data. Temperature-dependent electrical resistivity ρ (Figure 6, top), Seebeck coefficient *S* (Figure 6, middle), and thermal conductivity κ (Figure 6, bottom) in the temperature range from 10 to 700 K are shown in Figure 6. The agreement between the high- and low-temperature data, measured with two different setups on two different specimens, is an indication of the homogeneity of the materials prepared by SPS. Both materials $K_{7.6}Si_{46}$ and $K_{6.8}Si_{46}$ show metallic temperature dependence of ρ and *S*, in agreement with the seminal work by Cros et al. [6]. The fact that these materials show metallic conduction follows from the simple assertion that each K atom donates one electron to the silicon framework resulting in an overall high electron concentration. Measured ρ of cold-pressed $K_{7.6}Si_{46}$, obtained from the thermal decomposition of K_4Si_4, was reported to be much higher: $\rho \sim 140$ m$\Omega \cdot$ cm at room temperature with weak temperature dependence [28]. The large discrepancy between those results and the data shown in Figure 6 may be attributed to the microstructure of the specimens and the typically poor inter-granular contact that is achieved using cold pressing [28]. Nevertheless, the ρ values shown in Figure 6 are significantly larger than expected for the presumed high electron concentration. In addition, the residual resistance ratio, $\rho_{300K}/\rho_{10K} = 3.6$, is also relatively low for a good metal and significantly smaller than the values obtained for single crystals of Na_8Si_{46} ($\rho_{300K}/\rho_{10K} = 36$) [33] and $Na_{24}Si_{136}$ ($\rho_{300K}/\rho_{10K} = 14$) [17]. These results reiterate the need for high-density polycrystalline specimens in order to minimize the effects of grain boundary scattering on the transport properties of intermetallic clathrates [34].
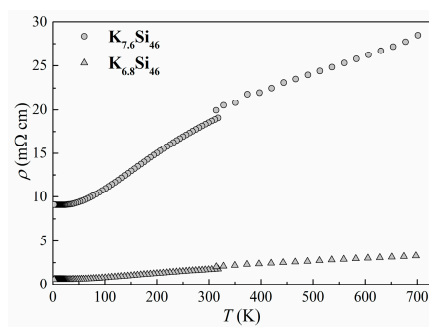
Figure 6. *Cont.*
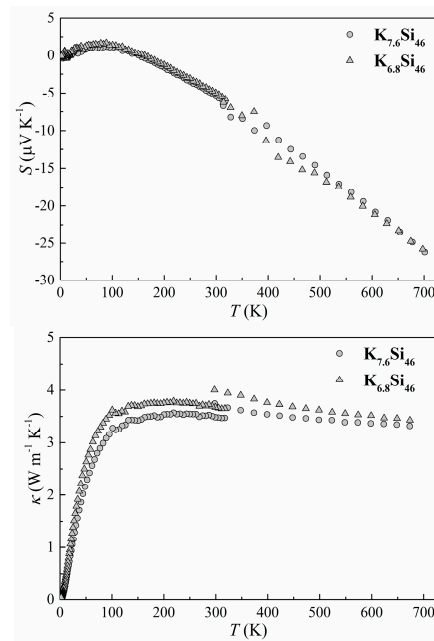
Figure 6. Transport properties of polycrystalline $K_{7.6}Si_{46}$ and $K_{6.8}Si_{46}$. The low temperature, 2 to 300 K, and high temperature, 300 to 700 K, are described in the text. (**Top**) electrical resistivity ρ; (**Middle**) Seebeck coefficient S; (**Bottom**) thermal conductivity κ.

3. Materials and Methods

3.1. Synthesis of Precursors

Binary precursors M_4Si_4 (M = Na, K, Rb, or Cs) were prepared from alkali metal pieces (ChemPur, Karlsruhe, Germany 99.9 wt %) and coarsely ground silicon (ChemPur, 99.999 wt %), by sealing of the precursor mixture under argon in small, welded tantalum ampoules that were enclosed under vacuum inside silica tubes and heated to 800 °C at an average rate of 3 °C/min. The ampoules were held at 800 °C for 4 h before being slowly cooled to room temperature (furnace cooled). The reaction products were determined to be single phase M_4Si_4 by powder X-ray diffraction (PXRD). All sample manipulations were performed in an argon-filled glove box (H_2O < 1 ppm; O_2 < 1 ppm). **CAUTION**: M_4Si_4 compounds are sensitive to air and moisture (pyrophoric) and must be kept under inert atmosphere at all times.

3.2. Spark Plasma Synthesis

SPS experiments were conducted under vacuum (background pressure <10 Pa) using a dedicated SPS setup in a protective argon atmosphere (Figure 2a; SPS: 515 ET, Syntex-Fuji, Japan; glove box: MBraun, Garching, Germany) [24]. Table 1 contains the preparation conditions for the clathrates synthesized within this study. The precursors were ground to fine powder and loaded into graphite or boron nitride (*h*-BN) dies with an inner diameter of 8 mm. Graphite or stainless steel punches were used to apply the uniaxial pressure. Tantalum foil was employed to surround the powder specimen on all sides, isolating the specimen from the die and punches during SPS processing. Graphite dies worked well for Na, however they were observed to react with alkali-metal vapor for precursors of K, Rb, and Cs and often cracked the graphite die during SPS processing. For these alkali metals *h*-BN was found to be most suitable. After SPS the products were isolated from the residual precursor by washing first with ethanol and then distilled water under flowing argon.

3.3. Sample Characterization

Powder X-ray diffraction (PXRD) data were collected using the Guinier technique (Huber G670 camera, Rimsting, Germany, Cu-$K_{\alpha1}$ radiation, $\lambda = 1.540598$ Å, graphite monochromator, $5° \leqslant 2\theta \leqslant 100°$, $\Delta 2\theta = 0.005°$). Crystal structure refinements were performed using the software WinCSD [25]. For the transport measurements, the $K_{7.6}Si_{46}$ and $K_{6.8}Si_{46}$ powders were first washed then consolidated by SPS using tungsten carbide tool (8 mm inner diameter) at 300 °C and a uniaxial pressure of 600 MPa under vacuum (background pressure of approximately 10 Pa) for 10 min. The density of the pellets was approximately 90% of the calculated density based on PXRD data. The specimens were cut with a diamond wire saw into parallelepiped pieces 1.5 mm × 1.5 mm × 8.0 mm for electrical transport measurements and low-temperature thermal conductivity measurements, and 1.5 mm thick and 8 mm in diameter disks for thermal diffusivity measurements. Electrical resistivity (ρ) and Seebeck coefficient (S) measurements from 22 to 450 °C on SPS densified $K_{7.6}Si_{46}$ and $K_{6.8}Si_{46}$ specimens were performed with a commercial ZEM-3 setup (ULVAC-RIKO, Munich, Germany). Specific heat (C_p) measurements were performed on a Netzsch Pegasus DSC (Selb, Germany) while heating to 450 °C at a heating rate of 10 °C/min in an Ar atmosphere. Thermal diffusivity, D, was measured from 22 °C to 450 °C using the laser-flash technique (LFA 457 Micro Flash, Netzsch, Selb, Germany). The temperature dependent thermal conductivity, κ, was calculated using the relation $\kappa = C_p \times D \times d$ where d is the density in g/cm^3. Low temperature ρ, S, and κ data were collected using the TTO-option (Thermal Transport Option) of a PPMS (Physical Property Measurement System) (Quantum Design, San Diego, CA, USA) using a four-point method.

4. Conclusions

Binary intermetallic clathrates $K_{8-x}Si_{46}$ ($x = 0.4$; 1.2), $Rb_{6.2}Si_{46}$, $Rb_{11.5}Si_{46}$, and $Cs_{7.8}Si_{136}$ were synthesized by spark plasma synthesis from the respective M_4Si_4 precursors. The formation of polycrystalline products at the anode of the SPS setup was observed for all compounds. The preparation of the new clathrate-II phase $Rb_{11.5}Si_{136}$ is further evidence that SPS is useful for the inorganic synthesis. The role the electric field is in driving the chemical conversion of the precursor into the clathrate phase at the anode during SPS processing is emphasized. Conventional thermal decomposition (CTC) [6,28,35], kinetically controlled thermal decomposition (KCTD) [18,19], chemical oxidation (CO) [7,27], and SPS yield different intermetallic clathrate phases from the same M_4Si_4 precursor (Table 4). While the influence of temperature clearly plays a role in clathrate formation, a definitive understanding of the local formation mechanisms in each of these synthetic approaches [36] is of great interest and is an ongoing task.

Table 4. Clathrate phases obtained by different synthesis techniques from M_4Si_4 precursors.

Precursor	Preparation Technique [a]	Clathrate Phases Obtained	References
Na_4Si_4	CTC	Na_8Si_{46} and $Na_{24-x}Si_{136}$	[6,33]
	KCTD	Na_8Si_{46} and $Na_{24-x}Si_{136}$	[18]
	CO	Na_8Si_{46} and $Na_{24-x}Si_{136}$	[7,25]
	SPS	Na_8Si_{46} and $Na_{24-x}Si_{136}$	[16,24], this work
K_4Si_4	CTC	$K_{8-x}Si_{46}$	[6,26]
	KCTD	$K_{8-x}Si_{46}$ and $K_{24-x}Si_{136}$	[19]
	CO	$K_{8-x}Si_{46}$	[7]
	SPS	$K_{8-x}Si_{46}$	this work
Rb_4Si_4	CTC	$Rb_{8-x}Si_{46}$	[6,26]
	SPS	$Rb_{8-x}Si_{46}$ and $Rb_{24-x}Si_{136}$	this work
Cs_4Si_4	CTC	$Cs_{24-x}Si_{136}$	[6]
	SPS	$Cs_{24-x}Si_{136}$	this work

[a] CO = chemical oxidation, KCTD = kinetically controlled thermal decomposition, CTC = conventional thermal decomposition, SPS = spark plasma synthesis.

Author Contributions: Y.G. and G.S.N. developed the concept of this study; I.V. and M.Be. conceived and designed the SPS experiments; I.A. and W.S. performed the physical measurements experiments; I.V., M.Be., and M.Ba. refined the crystal structures from PXRD experiments; all authors contributed to the text of the manuscript.

Conflicts of Interest: The authors declare no conflict of interest.

References

1. Hohmann, E. Silicide und Germanide der Alkalimetalle. *Z. Anorg. Chem.* **1948**, *257*, 113–126. [CrossRef]

2. Cros, C.; Pouchard, M.; Hagenmuller, P. Two new phases of the silicon-sodium system. *C. R. Hebd. Seances Acad. Sci.* **1965**, *260*, 4764–4767.

3. Cros, S.; Pouchard, M. Sur les phases de type clathrate du silicium et des éléments apparentés (C, Ge, Sn): Une approche historique. *C. R. Chim.* **2009**, *12*, 1014–1056. [CrossRef]

4. Nolas, G.S. (Ed.) *The Physics and Chemistry of Inorganic Clathrates*; Springer: Berlin, Germany, 2014.

5. Kasper, J.S.; Hagenmuller, P.; Pouchard, M.; Cros, C. Clathrate Structure of Silicon Na_8Si_{46} and Na_xSi_{136} (x < 11). *Science* **1965**, *150*, 1713–1714. [PubMed]

6. Cros, C.; Pouchard, M.; Hagenmuller, P. Sur une nouvelle famille de clathrates minéraux isotypes des hydrates de gaz et de liquides. Interprétation des résultats obtenus. *J. Solid State Chem.* **1970**, *2*, 570–581. [CrossRef]

7. Böhme, B.; Guloy, A.; Tang, Z.; Schnelle, W.; Burkhardt, U.; Baitinger, M.; Grin, Y. Oxidation of M_4Si_4 (M = Na, K) to Clathrates by HCl or H_2O. *J. Am. Chem. Soc.* **2007**, *129*, 5348–5349. [CrossRef] [PubMed]

8. Böhme, B.; Hoffmann, S.; Baitinger, M.; Grin, Y. Application of *n*-Dodecyltrimethylammonium Chloride for the Oxidation of Intermetallic Phases. *Z. Naturforsch.* **2011**, *66*, 230–238. [CrossRef]

9. Liang, Y.; Böhme, B.; Reibold, M.; Schnelle, W.; Schwarz, U.; Baitinger, M.; Lichte, H.; Grin, Y. Synthesis of the Clathrate-I Phase $Ba_{8-x}Si_{46}$ via Redox Reactions. *Inorg. Chem.* **2011**, *50*, 4523–4528. [CrossRef] [PubMed]

10. Krishna, L.; Chai, P.; Koh, C.A.; Toberer, E.S.; Nolas, G.S. Synthesis and structural properties of type I potassium SiGe alloy clathrates. *Mater. Lett.* **2015**, *149*, 123–126. [CrossRef]

11. Ammar, A.; Cros, C.; Pouchard, M.; Jaussaud, N.; Bassat, J.-M.; Villeneuve, G.; Duttine, M.; Ménétrier, M.; Reny, E. On the clathrate form of elemental silicon, Si_{136}: Preparation and characterisation of Na_xSi_{136} ($x \to 0$). *Solid State Sci.* **2004**, *6*, 393–400. [CrossRef]

12. Guloy, A.M.; Ramlau, R.; Tang, Z.; Schnelle, W.; Baitinger, M.; Grin, Y. A guest-free germanium clathrate. *Nature* **2006**, *443*, 320–323. [CrossRef] [PubMed]

13. Gallmeier, J.; Schäfer, H.; Weiss, A. Cage structure as a common building principle of compounds K_8E_{46} (E = silicon, germanium, tin). *Z. Naturforsch. B* **1969**, *24*, 665–667.

14. Bobev, S.; Sevov, S.C. Synthesis and Characterization of Stable Stoichiometric Clathrates of Silicon and Germanium: $Cs_8Na_{16}Si_{136}$ and $Cs_8Na_{16}Ge_{136}$. *J. Am. Chem. Soc.* **1999**, *121*, 3795–3796. [CrossRef]

15. Nolas, G.S.; Vanderveer, D.G.; Wilkinson, A.P.; Cohn, J.L. Temperature dependent structural and transport properties of the type II clathrates $A_8Na_{16}E_{136}$ (A = Cs or Rb and E = Ge or Si). *J. Appl. Phys.* **2002**, *91*, 8970–8973. [CrossRef]

16. Beekman, M.; Baitinger, M.; Borrmann, H.; Schnelle, W.; Meier, K.; Nolas, G.S.; Grin, Y. Preparation and Crystal Growth of $Na_{24}Si_{136}$. *J. Am. Chem. Soc.* **2009**, *131*, 9642–9643. [CrossRef] [PubMed]

17. Beekman, M.; Schnelle, W.; Borrmann, H.; Baitinger, M.; Grin, Y.; Nolas, G.S. Intrinsic Electrical and Thermal Properties from Single Crystals of $Na_{24}Si_{136}$. *Phys. Rev. Lett.* **2010**, *104*. [CrossRef] [PubMed]

18. Stefanoski, S.; Beekman, M.; Wong-Ng, W.; Zavalij, P.; Nolas, G.S. Simple Approach for Selective Crystal Growth of Intermetallic Clathrates. *Chem. Mater.* **2011**, *23*, 1491–1495. [CrossRef]

19. Stefanoski, S.; Nolas, G.S. Synthesis and Structural Characterization of Single-Crystal $K_{7.5}Si_{46}$ and $K_{17.8}Si_{136}$ Clathrates. *Cryst. Growth Des.* **2011**, *11*, 4533–4537. [CrossRef]

20. Baranowski, L.L.; Krishna, L.; Martinez, A.D.; Raharjo, T.; Stevanovic, V.; Tamboli, A.C.; Toberer, E.S. Synthesis and optical band gaps of alloyed Si–Ge type II clathrates. *J. Mater. Chem. B* **2014**, *2*, 3231–3237. [CrossRef]

21. Dong, Y.; Nolas, G.S. Rapid crystal growth of type-II clathrates $A_8Na_{16}Si_{136}$ (A = K, Rb, Cs) by spark plasma sintering. *Cryst. Eng. Commun.* **2015**, *17*, 2242–2244. [CrossRef]

22. Dong, Y.; Chai, P.; Beekman, M.; Zeng, X.; Tritt, T.M.; Nolas, G.S. Precursor Routes to Complex Ternary Intermetallics: Single-Crystal and Microcrystalline Preparation of Clathrate-I $Na_8Al_8Si_{38}$ from NaSi + NaAlSi. *Inorg. Chem.* **2015**, *54*, 5316–5321. [CrossRef] [PubMed]

23. Wei, K.; Dong, Y.; Nolas, G.S. Precursor routes to quaternary intermetallics: Synthesis, crystal structure, and physical properties of clathrate-II $Cs_8Na_{16}Al_{24}Si_{112}$. *J. Solid State Chem.* **2016**, *237*, 81–85. [CrossRef]

24. Reinfried, N.; Höhn, P.; Grin, Y. *Spark-Plasma Synthesis an Inert Gas Atmosphere*; Max-Planck-Institute for Chemical Physics of Solids: Dresden, Germany, 2006; p. 29.

25. Akselrud, L.; Grin, Y. WinCSD: Software package for crystallographic calculations (Version 4). *J. Appl. Crystallogr.* **2014**, *47*, 803–805. [CrossRef]

26. Stefanoski, S.; Blosser, M.C.; Nolas, G.S. Pressure Effects on the Size of Type-I and Type-II Si-Clathrates Synthesized by Spark Plasma Sintering. *Cryst. Growth Des.* **2013**, *13*, 195–197. [CrossRef]

27. Blosser, M.; Nolas, G.S. Synthesis of Na_8Si_{46} and $Na_{24}Si_{136}$ by oxidation of Na_4Si_4 from ionic liquid decomposition. *Mater. Lett.* **2013**, *99*, 161–163. [CrossRef]

28. Ramachandran, G.K.; McMillan, P.F.; Dong, J.; Sankey, O.F. $K_{7.62(1)}Si_{46}$ and $Rb_{6.15(2)}Si_{46}$: Two Structure I Clathrates with Fully Occupied Framework Sites. *J. Solid State Chem.* **2000**, *154*, 626–634. [CrossRef]

29. Bobev, S.; Sevov, S.C. Clathrates of Group 14 with Alkali Metals: An Exploration. *J. Solid State Chem.* **2000**, *153*, 92–105. [CrossRef]

30. Beekman, M.; Nenghabi, E.N.; Biswas, K.; Myles, C.W.; Baitinger, M.; Grin, Y.; Nolas, G.S. Framework Contraction in Na-Stuffed Si(*cF*136). *Inorg. Chem.* **2010**, *49*, 5338–5340. [CrossRef] [PubMed]

31. Shannon, R.D. Revised effective ionic radii and systematic studies of interatomic distances in halides and chalcogenides. *Acta Crystallogr. A* **1976**, *32*, 751–767. [CrossRef]

32. Reny, E.; Gravereau, P.; Cros, C.; Pouchard, M. Structural characterisations of the Na_xSi_{136} and Na_8Si_{46} silicon clathrates using the Rietveld method. *J. Mater. Chem.* **1998**, *8*, 2839–2844. [CrossRef]

33. Stefanoski, S.; Martin, J.; Nolas, G.S. Low temperature transport properties and heat capacity of single-crystal Na_8Si_{46}. *J. Phys. Condens. Matter* **2010**, *22*. [CrossRef] [PubMed]

34. Beekman, M.; Nolas, G.S. Transport Properties of the Binary Type I Clathrate $K_8Ge_{44}\square_2$. *Int. J. Appl. Ceram. Technol.* **2007**, *4*, 332–338. [CrossRef]

35. Cros, C.; Benejat, J.-C. Preparation and properties of a clathrate having an extensive domain of existence. Sodium silicide Na_xSi_{136} compounds. *Bull. Soc. Chim. Fr.* **1972**, *5*, 1739–1743.

36. Hutchins, P.T.; Leynaud, O.; O'Dell, L.A.; Smith, M.E.; Barnes, P.; McMillan, P.F. Time-Resolved in Situ Synchrotron X-ray Diffraction Studies of Type 1 Silicon Clathrate Formation. *Chem. Mater.* **2011**, *23*, 5160–5167. [CrossRef]